

# Flow separation characteristics of supersonic nozzles in water environment

*Deyou Wang\*, Ge Jin\*, Ruyao Wang\* and Shipeng Li\*†*

*\* School of Aerospace Engineering, Beijing Institute of Technology  
No. 5, South Street, Zhongguancun, Haidian District, Beijing, 100081, China  
wangdeyou10000@163.com – jinge52293@163.com – ruyaowang@163.com*

*† Corresponding Author: lsp@bit.edu.cn*

## Abstract

An experimental system is established to investigate the flow separation characteristics of a supersonic planar nozzle in water environment. The intermittent reciprocating motions of separation shock, the tilt of jet patterns caused by asymmetric separation and the side-to-side swings of the jet axis have been observed. Furthermore, the separated flow of an over-expanded parabolic nozzle operating in water is numerically studied. The gas-liquid separation accompanied by shock-induced flow separation has been observed in the nozzle. It is found that there are transitions between different flow separation patterns, and the separation point is continuously oscillating. These phenomena are attributed to pressure fluctuations caused by the unsteady behavior of the gas-liquid interface.

## 1. Introduction

Jet propulsion with supersonic nozzles is the main propulsion method for rockets and spacecrafts. Its application in underwater vehicles is being further discussed, which can provide more possibilities for propulsion of trans-media vehicles and underwater launched rockets. For a supersonic nozzle with a definite area ratio, flow separation from the nozzle wall may occur when the ratio of inlet pressure to ambient pressure (nozzle pressure ratio, NPR) is small. This usually occurs during the transient startup and shutdown of the engine. Due to the interaction between shocks and near-wall turbulence inside the nozzle, the separated flow usually exhibits a strong unsteadiness and sometimes a loss of symmetry, resulting in dangerous side loads. To achieve better performance, larger nozzle area ratio and wider depth adaptation range are the future trends for underwater jet propulsion. The consequent problem of flow separation for supersonic nozzles in water environment needs to be paid more attention by researchers.

For underwater jet propulsion, Moon et al. [1] conducted static tests of a laboratory-scale hybrid rocket motor in a water tank and evaluated the performance of the motor. Gupta et al. [2-3] designed a submerged combustor for the propulsion requirements of future autonomous underwater vehicles (AUVs), and analyzed the structure, behavior and dynamics of the exhaust jets. Unlike in air, the supersonic gas jets submerged in water are highly turbulent and unstable, primarily due to the velocity shear and density differences between the gas-liquid phases, as well as the shock/jet interface interactions. Loth et al. [4] conducted experiments on the structure of planar under-expanded air jets in a water tank. The flow visualization indicated the presence of shock-containing external expansion regions, which decay more rapidly than air-to-air jets due to the intense gas-liquid mixing. Shi et al. [5-6] conducted a series of experimental studies on the oscillation flow characteristics of underwater supersonic gas jets exhausted from Laval nozzles in a water tank. The flow pattern during the jet development and the jet expansion feedback phenomenon were analyzed in detail. Weiland et al. [7] evaluated the pinch-off location, penetration distance and unsteady interface characteristics of underwater round supersonic gas jets through experiments. Due to the limited information of flow field obtained from experiments, numerical simulation based on computational fluid dynamics (CFD) has gradually become an important method to study the flow characteristics. Many numerical simulations based on the volume of fluid (VOF) multiphase model have been conducted to investigate the flow mechanism and thrust performance of the supersonic gas jets for underwater propulsion. Moreover, the effects of water depth, pressure ratio, nozzle area ratio, and ambient fluid density have been analyzed [8-11].

Previous studies on underwater jet propulsion focus mainly on the flow dynamics and oscillations of the underwater gas jets, where the pressure ratio is relatively high and the nozzle area ratio is small. For large area ratio nozzles in highly over-expanded states, flow separation is usually inevitable. Many experimental and numerical studies have been conducted on the mechanism of unsteady flow separation in rocket engine nozzles with specific profiles in air [12-15].

The phenomena of free shock separation (FSS) and restricted shock separation (RSS) have been observed. Moreover, the behavior of separated and reattached shocks as well as the origin of side loads have been analyzed in detail. For nozzles operating in water environment, Ferguson [16] conducted experiments in a horizontal pressure vessel in the 1960s at simulated depths greater than 200 m. A 15° half-angle conical nozzle made of Lucite was used in the experiments, and the oscillations of the separation plane in the nozzle were observed. However, there have been very few subsequent studies on the flow separation characteristics of supersonic nozzles in water environment.

In this paper, a highly visualized experimental system of underwater planar vertical gas jets is established. The basic characteristics of flow separation for supersonic nozzles in water environment are discussed. To further reveal the mechanism of flow separation for underwater propulsion, the flow process of an over-expanded parabolic nozzle operating at a water depth of 50 m is numerically studied. The unsteady motions of shock and separation point, and the fluctuations of wall-pressure distribution in the nozzle are analyzed in detail. The differences of flow separation characteristics in water and air under the same pressure ratio are also compared.

## 2. Experimental methods

Figure 1 shows the schematic diagram of the experimental setup. The facility consists of a rectangular water tank, gas supply system, illumination system and measuring system. The water tank with dimensions (length  $\times$  width  $\times$  height) 1000 mm  $\times$  400 mm  $\times$  800 mm, has transparent sidewalls made of PMMA for optical measurements. The water depth in the tank is 750 mm. Compressed air stored in a gas cylinder is used as the gas source. A pressure reducing valve is arranged in the pipeline to adjust the gas pressure, and a solenoid valve is used to control the gas injection. Johnson and Papamoschou [18] have studied the instability of shock-induced flow separation in an over-expanded supersonic planar nozzle, in which the unsteady shock behavior has been effectively observed. Inspired by the experimental study in Ref. [4] and [18], a set of planar nozzle assembly is designed. The planar nozzle made of stainless steel is installed on the bottom base of the tank. It has a throat width of 1 mm, an outlet width of 2 mm and a slot depth of 10 mm. The area ratio of the nozzle is 2, therefore, the designed outlet Mach number obtained by theoretical calculation is 2.2. To improve the observation of flow state inside the nozzle and near the outlet, the planar nozzle is clamped by two PMMA plates with a spacing of 10 mm.

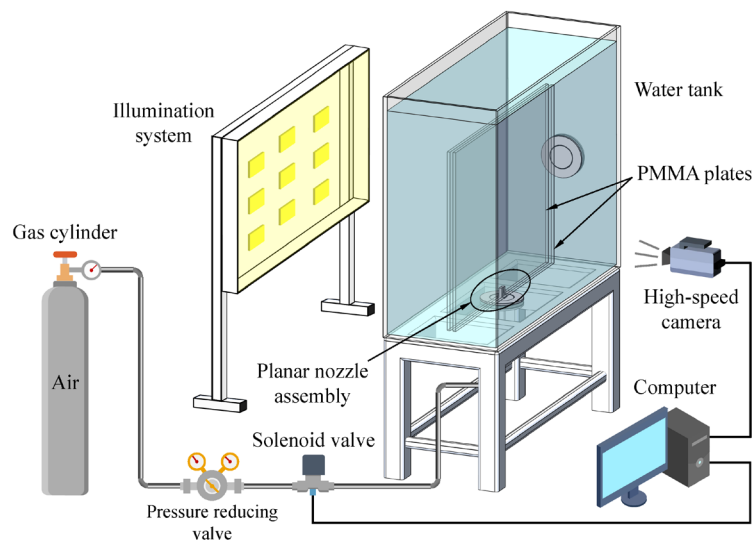


Figure 1: Schematic diagram of the experimental setup

The structures of the experimental rectangular water tank and the planar nozzle are shown in Figure 2. When the solenoid valve is triggered to open, high-pressure air is injected vertically upwards into the water through the planar nozzle. A high-speed camera (Phantom VEO 710S) is used to record the flow process of the gas injection near the nozzle. The recording frequency is 5000 frames per second. The background illumination is provided by a white-light lamp bank, which is installed on the back side of the water tank. The illumination system, the high-speed camera, and the computer are combined to form the basis for the flow visualization technique.



(a) Rectangular water tank

(b) Planar nozzle

Figure 2: Structure of the experimental device

### 3. Numerical simulation methods

#### 3.1 Governing equations

The flow process for an over-expanded supersonic nozzle in water environment is an unsteady, compressible and multiphase flow process. The simulation involves complex issues such as shock-shock interactions, gas-liquid interface tracking and turbulent boundary layer separation. In this study, air is treated as a single-component compressible ideal gas, and liquid water is treated as an incompressible fluid. Based on the understanding of the above issues, the basic governing equations can be described as follows:

Mass conservation equation:

$$\frac{\partial \rho}{\partial t} + \nabla \cdot (\rho \mathbf{u}) = 0 \quad (1)$$

where,  $\rho$  is the density of the mixture, and it can be defined as  $\rho = \alpha_1 \rho_1 + \alpha_2 \rho_2$ . Here,  $\rho_1$  and  $\rho_2$  are the density of air and water, respectively;  $\alpha_1$  and  $\alpha_2$  are the volume fraction of air and water, respectively.  $\mathbf{u}$  is velocity vector.

Momentum conservation equation:

$$\frac{\partial}{\partial t}(\rho \mathbf{u}) + \nabla \cdot (\rho \mathbf{u} \mathbf{u}) = -\nabla p + \nabla \cdot \boldsymbol{\tau} \quad (2)$$

where,  $p$  is the fluid pressure in the flow field,  $\boldsymbol{\tau}$  is the stress tensor. The expression of  $\boldsymbol{\tau}$  is as follows:

$$\boldsymbol{\tau} = \mu \left[ (\nabla \mathbf{u} + \nabla \mathbf{u}^T) - \frac{2}{3} (\nabla \cdot \mathbf{u}) \mathbf{I} \right] \quad (3)$$

where,  $\mu$  is the viscosity of the mixture, and it can similarly be defined as  $\mu = \alpha_1 \mu_1 + \alpha_2 \mu_2$ ;  $\mathbf{I}$  is the unit tensor.

Energy conservation equation:

$$\frac{\partial}{\partial t}(\rho E) + \nabla \cdot [\mathbf{u}(\rho E + p)] = \nabla \cdot [\lambda_{\text{eff}} \nabla T + (\boldsymbol{\tau}_{\text{eff}} \cdot \mathbf{u})] \quad (4)$$

where,  $E$  and  $T$  are the energy and temperature of the mixture, respectively;  $\lambda_{\text{eff}}$  is the effective thermal conductivity. Here,  $E$  and  $T$  are treated as mass averaged variables, and the value of them are calculated by following relations:

$$E = \frac{\sum_{q=1}^2 \alpha_q \rho_q E_q}{\sum_{q=1}^2 \alpha_q \rho_q}, T = \frac{\sum_{q=1}^2 \alpha_q \rho_q T_q}{\sum_{q=1}^2 \alpha_q \rho_q} \quad (5)$$

Gas state equation:

$$p = \rho_1 R T \quad (6)$$

where  $R$  is the gas constant of air.

### 3.2 VOF multiphase model

The gas-liquid interface is captured using the VOF multiphase model, in which the volume fraction of each of the fluids in each computational cell is tracked throughout the computational domain and the volume fraction is also a variable of the flow field. For the simulation of the underwater supersonic gas jets, the validity of the VOF model has been verified in Ref. [8-11]. For the phase  $q$ , the volume fraction equation has the following form:

$$\frac{\partial}{\partial t}(\alpha_q \rho_q) + \nabla \cdot (\alpha_q \rho_q \mathbf{u}_q) = S_{\alpha_q} + \sum_{p=1}^n (\dot{m}_{pq} - \dot{m}_{qp}) \quad (7)$$

where,  $\alpha_q$ ,  $\rho_q$  and  $\mathbf{u}_q$  are the volume fraction, density and velocity of phase  $q$ , respectively;  $S_{\alpha_q}$  is the source term of phase  $q$ ;  $\dot{m}_{pq}$  is the mass transfer from phase  $p$  to phase  $q$ ,  $\dot{m}_{qp}$  is the mass transfer from phase  $q$  to phase  $p$ . The phase volume fraction is constrained by the following expression:

$$\sum_{q=1}^n \alpha_q = 1 \quad (8)$$

In this study, air is defined as the primary phase and liquid water is defined as the secondary phase. Both two phases have no additional generated sources, and the mass transfer between them is ignored, *i.e.*, the right-hand of the phase volume fraction conservation equation is zero. The density of liquid water is  $998.2 \text{ kg m}^{-3}$  and its dynamic viscosity is  $1.003 \times 10^{-3} \text{ Pa s}$ .

### 3.3 Turbulence model

The two-equation SST  $k$ - $\omega$  turbulence model is used to close the Reynolds-averaged Navier-Stokes equations. The model is more accurate in the aspects of adverse pressure gradient flows and transonic shocks capturing. The transport equations for the turbulence kinetic energy  $k$  and the specific dissipation rate  $\omega$  are described as follows:

$$\frac{\partial}{\partial t}(\rho k) + \frac{\partial}{\partial x_i}(\rho k u_i) = \frac{\partial}{\partial x_j} \left( \Gamma_k \frac{\partial k}{\partial x_j} \right) + G_k - Y_k + S_k \quad (9)$$

$$\frac{\partial}{\partial t}(\rho \omega) + \frac{\partial}{\partial x_i}(\rho \omega u_i) = \frac{\partial}{\partial x_j} \left( \Gamma_\omega \frac{\partial \omega}{\partial x_j} \right) + G_\omega - Y_\omega + D_\omega + S_\omega \quad (10)$$

where,  $G_k$  represents the production of turbulence kinetic energy,  $G_\omega$  represents the generation of  $\omega$ ;  $\Gamma_k$  and  $\Gamma_\omega$  represent the effective diffusivity of  $k$  and  $\omega$ , respectively;  $Y_k$  and  $Y_\omega$  represent the dissipation of  $k$  and  $\omega$  due to turbulence;  $D_\omega$  represents the cross-diffusion term;  $S_k$  and  $S_\omega$  are user-defined source terms.

### 3.4 Computational domain and simulation setup

In order to discuss the characteristics of flow separation in practical underwater propulsion, a subscale parabolic nozzle is selected for numerical simulation. The basic calculation parameters of the nozzle are shown in Table 1. It is assumed that the nozzle outlet is equipped with a sealing cover that can be opened instantly to prevent the ingress of ambient water.

A computational domain containing the nozzle and the external environment is constructed, as shown in Figure 3. Considering the axial symmetry of the physical model, a two-dimensional axisymmetric model is used for numerical simulation. To exclude the influence of boundaries on the flow in the core region, the total length and total width of the computational domain are 240 times and 60 times the nozzle throat radius  $R_t$ , respectively. The nozzle inlet is defined as a pressure inlet boundary, with a total pressure of 6 MPa and a total temperature of 450 K. The left, upper and right boundaries of the external flow domain are defined as pressure outlet boundaries. The outlet pressure is the hydrostatic pressure corresponding to the water depth, and the ambient temperature is 300 K. All other walls are defined as non-slip adiabatic wall boundaries. Initially, the entire nozzle is filled with static gas at a pressure of 6 MPa.

Table 1: Basic calculation parameters of the nozzle

Parameter	Value
Area ratio $\varepsilon$	12.96
Nozzle length $L$ , mm	80
Throat diameter $D_t$ , mm	20
Normalized inlet wall radius $R_{td}/R_t$	0.5
Throat wall angle $\theta_N$ , $^\circ$	30
Nozzle exit angle $\theta_E$ , $^\circ$	5
Nozzle exit diameter $D_e$ , mm	72
Design feeding pressure $p_0$ , MPa	6
Design feeding temperature $T_0$ , K	450
Feeding gas	Air

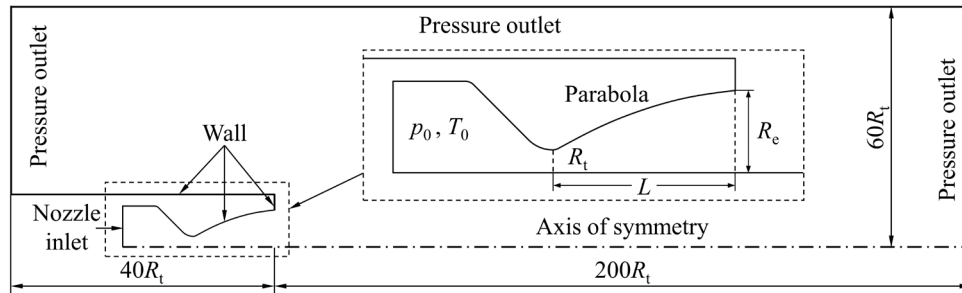


Figure 3: Computational domain and boundary conditions

A structured mesh is used for simulation. To better capture the shear layer and shock cell structure, the mesh is refined in regions with high gradients, such as the nozzle throat, divergent section and jet core. The overall computational mesh and the local grid near the nozzle are shown in Figure 4. The total cell number of the mesh is about 195000. The  $y^+$  of the first grid point on the nozzle wall is less than 5, which meets the requirements of the selected turbulence model.

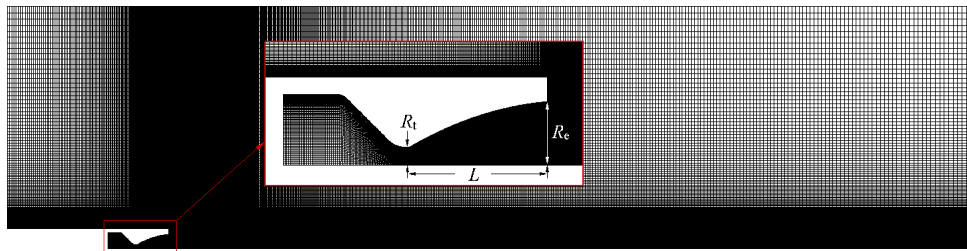


Figure 4: Computational mesh

The finite volume method is adopted to solve the governing equations. The coupling velocity and pressure equations are solved with the PISO algorithm. The discretization of gradient in space is undertaken using a least squares cell-based scheme, and the body force weighted scheme is used in the pressure term. The density and momentum terms follow a second-order upwind scheme, and the QUICK scheme is used for the phase volume fraction. The time discretization term is based on the first order implicit scheme. A time step of  $1 \times 10^{-6}$  s is chosen for calculation.

In this study, two operating conditions with the same NPR of 10 have been simulated, as shown in Table 2. The operating ambient medium are water and air respectively. In Case-1, the ambient pressure  $p_a$  is set to 0.6 MPa to simulate the water environment at a depth of 50 m. Case-2 is used as the control group to analyze the influence of ambient medium on flow separation characteristics.

Table 2: Operating conditions of the simulation cases

Case	$p_0$ , MPa	$p_a$ , MPa	Ambient medium
Case-1	6	0.6	Water
Case-2	6	0.6	Air

## 4. Results and discussion

### 4.1 Experimental results of the planar nozzle

The experimental results under a typical operating condition are analyzed, in which the inlet pressure of the planar nozzle is set to 0.4 MPa. The water depth above the nozzle outlet in the tank is about 700 mm, which will generate an additional pressure increment of 0.07 MPa, so the NPR is about 3.74. The nozzle operates in a highly over-expanded state, resulting in shock formation and shock/boundary layer interaction inside the nozzle. The evolution of flow patterns near the nozzle outlet obtained by the experimental photography is shown in Figure 5, where the time in Figure 5(a) is taken as the time origin. It can be seen that the over-expanded planar gas jets in water have strong unsteady characteristics. Due to the complex gas-liquid interaction, the jet boundary near the nozzle outlet is continuously expanding and contracting. The behavior of the jet shows similar characteristics to that of an underwater over-expanded round gas jet, including bulging, necking, pinch-off and back-attack.

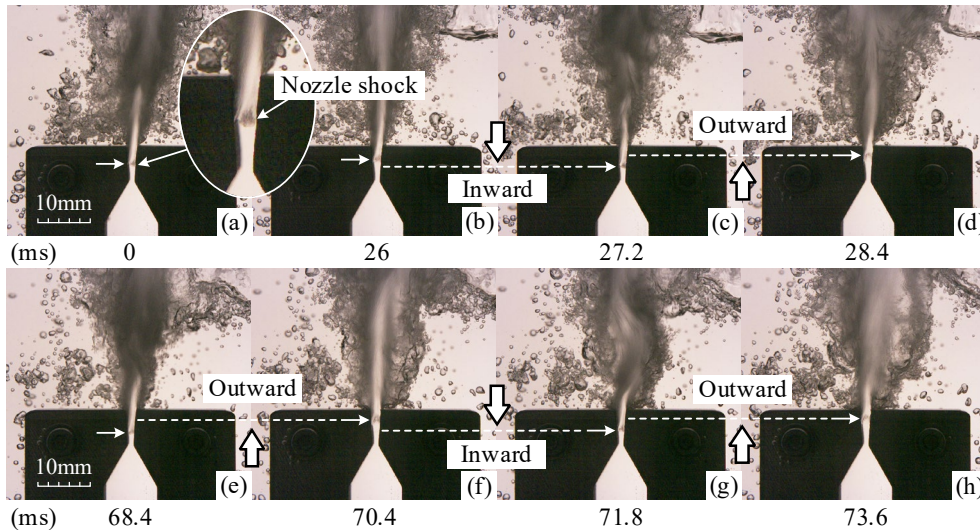


Figure 5: Evolution of flow patterns near the nozzle outlet

Due to the highly visualized design, the flow state of the airflow inside the nozzle and near the outlet can be clearly observed. However, in the downstream of the jet with lower velocity, the bubble groups resulting from the intense gas-liquid mixing leads to the decrease of visibility. It can be seen from the experimental results that the shock-induced flow separation occurs in the nozzle. It should be noted that the gas-liquid separation also occurs after the shock separation point, indicating the entry of external water into the nozzle divergent section. In air, it has been demonstrated that the interaction of the shock with the turbulent fluid near the nozzle wall can cause shedding of the vortex structures, leading to unsteadiness of the shock position and the downstream flow [17]. The oscillations of separation shock have also been observed in a shock-containing planar nozzle [18]. In water environment, the flow in the separation zone after the shock is disturbed by liquid droplets. The continuous expansion and contraction of the jet interface outside the nozzle lead to fluctuations of the pressure field. As a result, the separation shock undergoes

high-frequency small oscillations. In addition, the intermittent unsteady behavior of the jet (pinch-off and back-attack) will result in large fluctuations in outlet pressure, causing large piston-like reciprocating motions of the separation shock. Several cycles of the inward and outward motion of the shock are shown in Figure 5.

Figure 6 shows the flow patterns of the planar gas jet at different times. It is clear that the axis of the jet core tilts to the left or right. This is because that the flow separation in the nozzle is not always symmetrical due to the instability of the gas-liquid interaction. The uneven distribution of nozzle wall pressure caused by asymmetric separation will lead to a tilted macroscopic pattern of the jet, resulting in serious problems of thrust instability and thrust eccentricity. Similar phenomena have also been observed for the shock-containing nozzle in air [18]. But differently, the underwater planar gas jet undergoes intermittent side-to-side swings, and the switches in direction are almost instantaneous. This phenomenon can be attributed to the triggering of the jet bubble behavior, and there is a certain randomness in the switching of the tilt direction.

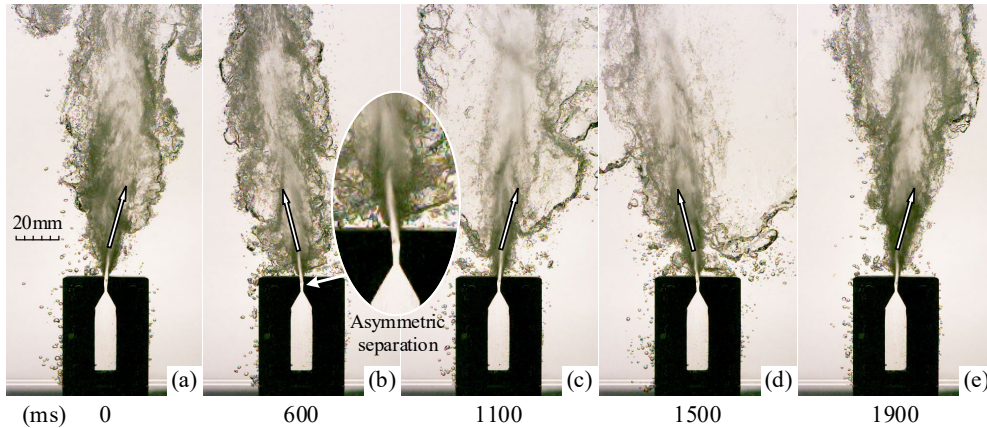


Figure 6: Flow patterns of the planar gas jet at different times

#### 4.2 Simulation results of the parabolic nozzle

The simulation results under different ambient medium are analyzed and compared. Figure 7 shows the evolution of bubble morphology for the parabolic nozzle operating in water through the contours of gas volume fraction  $\alpha_g$ . It can be seen that the jet structure contains a gas bag on the top and a gas passage with unsteady interfaces. As the gas continues to fill, the bubble is gradually elongated and moves downstream. Under the blocking effect of high-density water, the momentum of gas decays rapidly. The downstream bubbles are not strong enough to resist the ambient high pressure, resulting in irregular collapse of the morphology. Due to the instability of high-speed gas-liquid shear flow, unstable turbulent mixing and entrainment occur at the phase interfaces. Under the interaction of shocks and unsteady gas-liquid interfaces, the jet boundary near the nozzle outlet shows regular bulging and necking. Moreover, the jet pinch-off event and the process of water entering the nozzle are also observed, as shown in Figure 7(d) and (e).

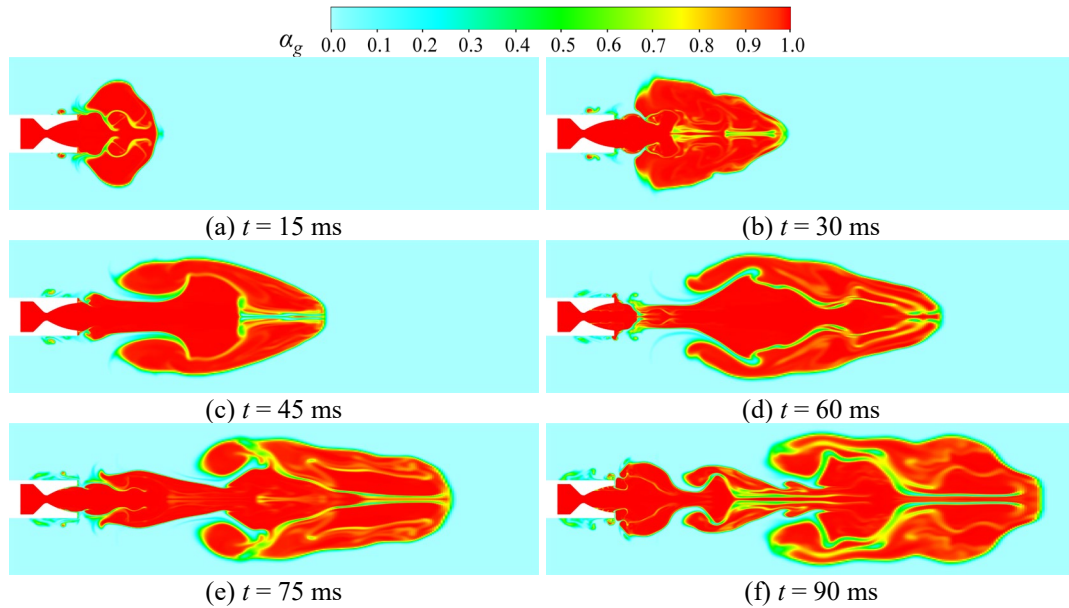


Figure 7: Evolution of bubble morphology for the parabolic nozzle operating in water

Figure 8 shows the distributions of Mach number and pressure near the nozzle outlet at  $t = 100$  ms in air. It can be seen that the boundary layer separates from the nozzle wall and never reattaches, and the separated flow continues as a free jet. It is clear that a typical FSS pattern occurs in the nozzle. Due to the constant inlet pressure, the flow tends to be stable and the position of separation point tends to be fixed. The separation point is close to the throat, indicating that the nozzle is in a highly over-expanded state.

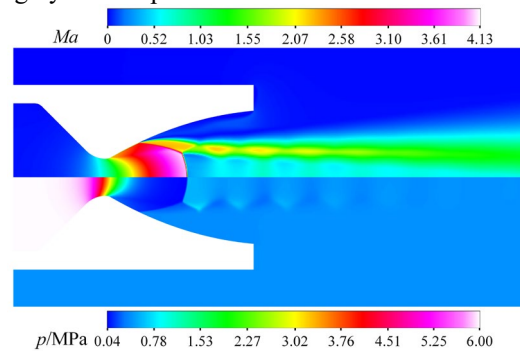


Figure 8: Flow field near the nozzle outlet at  $t = 100$  ms in air

Figure 9 shows the distributions of Mach number and pressure near the nozzle outlet at different times in water. Moreover, the interface of two phases is plotted by iso-volume of gas fraction  $\alpha_g$  of 0.7, which is also used as the dividing parameter of gas-water interface in Ref. [10]. It is obvious that the shock structure and flow separation pattern in the nozzle are strongly unsteady. As can be seen from Figure 9(a), (b) and (f), the RSS pattern occurs in the nozzle, where the separated flow reattaches to the nozzle wall, thereby forming a closed recirculation bubble. However, the FSS pattern is observed in Figure 9(c), (d) and (e). It can be concluded that there are transitions between different flow separation patterns in the parabolic nozzle operating in water, and the position of the separation point is continuously oscillating. These are attributed to the pressure field fluctuations caused by the unsteady behavior of the jet boundary near the nozzle outlet. Therefore, although the nozzle inlet pressure and ambient water depth are fixed, the actual NPR is constantly changing. As shown in Figure 9(d), the high pressure caused by jet pinch-off makes the separation point very close to the nozzle throat.

It should be noted that, according to the simulation results, the external water will not always remain in the divergent section. This is different from the experimental results of the planar nozzle. It indicates that there are two types of separation in the nozzle, namely shock-induced gas flow separation and gas-liquid separation. When a large jet necking causes water to enter the nozzle, only the FSS pattern will occur, and the shock-induced separation point is the location of gas-liquid separation, as shown in Figure 9(e). However, this does not strictly conform to the typical definition of FSS, as in this case, the gas-liquid interface plays the role of the wall.

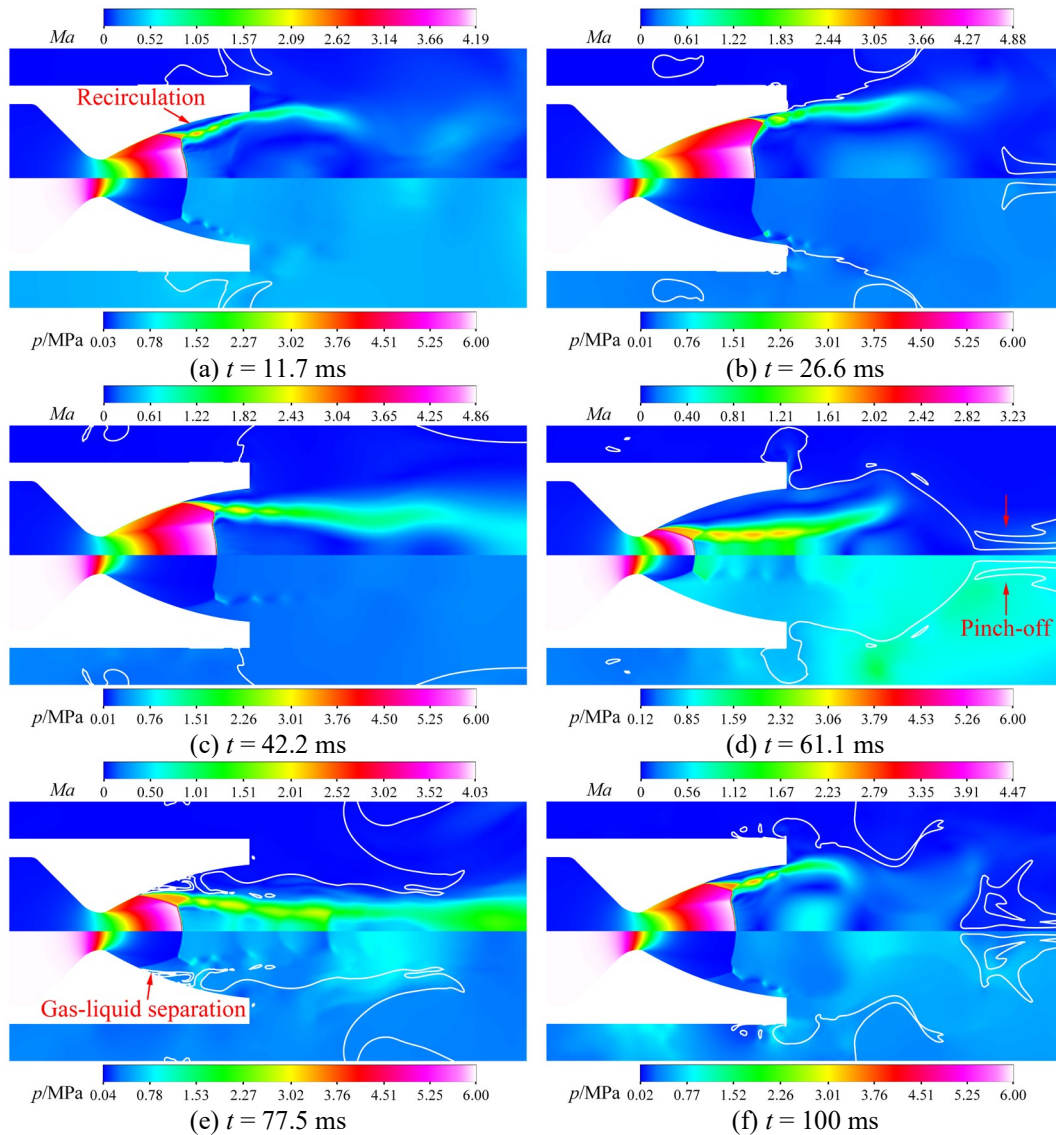


Figure 9: Flow field near the nozzle outlet at different times in water

The wall-pressure distributions corresponding to different times in Figure 9 are analyzed. Figure 10 shows the comparison of normalized wall-pressure distributions in air and water. It can be seen from Figure 10(a) that the wall-pressure before the separation point in air decreases with the expansion of airflow. While after the separation point, the pressure increases rapidly and tends to the ambient pressure. It can be seen from Figure 10(b) that the wall pressure distribution varies greatly at different times in water. At  $t = 11.7$  ms, 26.6 ms and 100 ms, the wall-pressure distributions in water basically follow the general pattern of RSS in air [19]. At  $t = 42.2$  ms, the normalized wall-pressure after the separation point is around 0.6, and at  $t = 61.1$  ms it is around 1.5. The results are different from the general pattern of FSS in air. At  $t = 77.5$  ms, due to the interaction between shocks and water in the divergent section, local rise and fall have appeared in the pressure platform after the separation point.

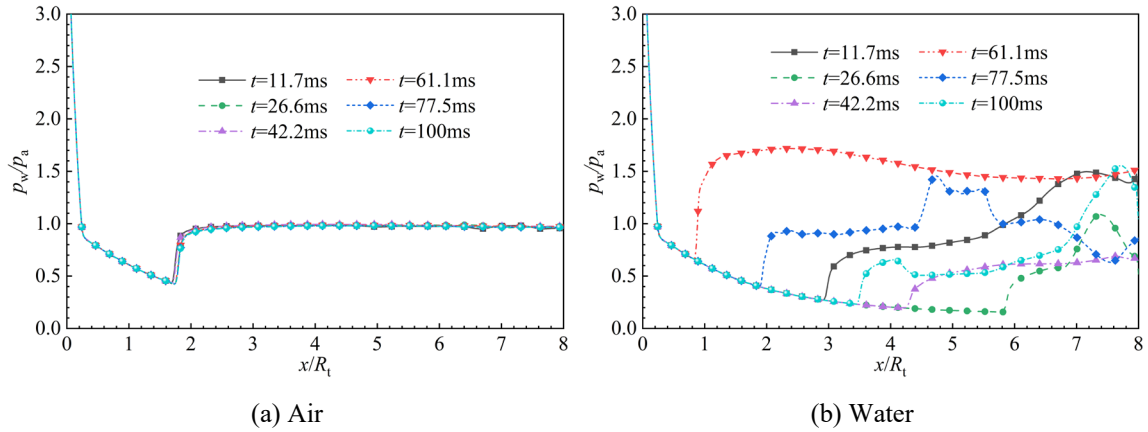


Figure 10: Comparison of normalized wall-pressure distributions in air and water

The nozzle thrust can be calculated by integrating the pressure on the internal and external walls. Due to the limitations of axisymmetric model, the side loads cannot be obtained. A comparison of nozzle thrust in air and water is shown in Figure 11, where the thrust peak at  $t = 0$  ms is caused by the initial high-pressure gas filling of the nozzle. It can be seen that the nozzle thrust in air quickly reaches stability within about 10 ms. However, due to the unsteady shock motions inside the nozzle and the fluctuations of wall-pressure, the nozzle thrust in water is continuously oscillating, and the average thrust is lower than that in air.

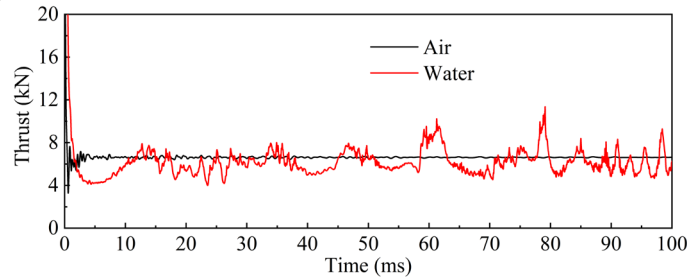


Figure 11: Comparison of nozzle thrust in air and water

## 5. Conclusions

With the experimental observations of underwater planar gas jets, and the numerical simulations of separated flow in a parabolic nozzle, the main conclusions can be summarized as follows:

- (1) The over-expanded gas jets in water have strong unsteady characteristics. The shock-induced flow separation occurs in the planar nozzle, and the gas-liquid separation also occurs after the shock separation point. Due to the complex gas-liquid interaction, the separation shock undergoes high-frequency small oscillations with intermittent large reciprocating motions. The asymmetric separation in the nozzle leads to a tilted macroscopic pattern of the jet, accompanied by intermittent side-to-side swings.
- (2) There are transitions between different flow separation patterns (FSS $\leftrightarrow$ RSS) in the parabolic nozzle operating in water, and the position of separation point is continuously oscillating. These are attributed to the pressure field fluctuations caused by the unsteady behavior of the gas-liquid interface. There are two types of separation in the nozzle, namely shock-induced gas flow separation and gas-liquid separation. When a large jet necking causes water to enter the nozzle, only the FSS pattern will occur, and the shock-induced separation point is the location of gas-liquid separation.
- (3) In the case of RSS, the wall-pressure distributions of the nozzle in water basically follow the general pattern of RSS in air. While in the case of FSS, unlike the general pattern of FSS in air, the wall-pressure after the separation point no longer tends to the ambient pressure. Due to the unsteady shock motions inside the nozzle and the fluctuations of wall-pressure, the nozzle thrust in water is continuously oscillating, and the average thrust is lower than that in air.

## References

- [1] H. Moon, S. Han, Y. You, and M. Kwon. 2019. Hybrid rocket underwater propulsion: a preliminary assessment. *Aerospace*. 6(3):28.
- [2] M. Linck, A. K. Gupta, and K. Yu. 2009. Submerged combustion and two-phase exhaust jet instabilities. *J. Propuls. Power*. 25(2):522–532.
- [3] V. K. Arghode, and A. K. Gupta. 2012. Jet characteristics from a submerged combustion system. *Appl. Energy*. 89:246–253.
- [4] E. Loth, and G. M. Faeth. 1990. Structure of plane underexpanded air jets into water. *AIChE J.* 36(6):818–826.
- [5] H. Shi, B. Wang, and Z. Dai. 2010. Research on the mechanics of underwater supersonic gas jets. *Sci. China Physics, Mech. Astron.* 53(3):527–535.
- [6] H. Shi, Q. Guo, C. Wang, R. Dong, L. Zhang, H. Jia, X. Wang, and B. Wang. 2010. Oscillation flow induced by underwater supersonic gas jets. *Shock Waves*. 20:347–352.
- [7] C. Weiland, and P. P. Vlachos. 2013. Round gas jets submerged in water. *Int. J. Multiph. Flow*. 48:46–57.
- [8] J. Tang, N. Wang, and W. Shyy. 2011. Flow structures of gaseous jets injected into water for underwater propulsion. *Acta Mech. Sin.* 27(4):461–472.
- [9] M. Fronzo, and M. Kinzel. 2016. An investigation of compressible gas jets submerged into water. In: *46th AIAA Fluid Dynamics Conference*. 4253.
- [10] X. Zhang, S. Li, B. Yang, and N. Wang. 2020. Flow structures of over-expanded supersonic gaseous jets for deep-water propulsion. *Ocean Eng.* 213:107611.
- [11] A. Jana, L. Hoskoti, and M. M. Sucheendran. 2022. A numerical study of the flow field driven by a submerged, high-speed, gaseous jet. *J. Fluids Eng.* 144:111208.
- [12] A. T. Nguyen, H. Deniau, S. Girard, and T. Alziary de Roquefort. 2003. Unsteadiness of flow separation and end-effects regime in a thrust-optimized contour rocket nozzle. *Flow, Turbul. Combust.* 71:161–181.
- [13] S. B. Verma, R. Stark, and O. Haidn. 2006. Relation between shock unsteadiness and the origin of side-loads inside a thrust optimized parabolic rocket nozzle. *Aerosp. Sci. Technol.* 10:474–483.
- [14] S. B. Verma, and O. Haidn. 2009. Study of restricted shock separation phenomena in a thrust optimized parabolic nozzle. *J. Propuls. Power*. 25(5):1046–1057.
- [15] A. Hadjadj, Y. Perrot, and S. Verma. 2015. Numerical study of shock/boundary layer interaction in supersonic overexpanded nozzles. *Aerosp. Sci. Technol.* 42:158–168.
- [16] J. D. Ferguson. 1969. Experimental data from underwater conical nozzles exhausting N<sub>2</sub> gas. *J. Hydronautics*. 3(4):200.
- [17] B. Olson, and S. Lele. 2013. A mechanism for unsteady separation in over-expanded nozzle flow. *Phys. Fluids*. 25:110809.
- [18] A. Johnson, and D. Papamoschou. 2010. Instability of shock-induced nozzle flow separation. *Phys. Fluids*. 22:016102.
- [19] M. Frey, and G. Hagemann. 1999. Flow separation and side-loads in rocket nozzles. In: *35th Joint Propulsion Conference and Exhibit*. 2815.